Research Square

Preprints are preliminary reports that have not undergone peer review.
They should not be considered conclusive, used to inform clinical practice,
or referenced by the media as validated information.

Reaction-driven ionic remodeling enables durable soft electronics

Do Hwan Kim

dhkim76@hanyang.ac.kr

Hanyang University https://orcid.org/0000-0003-3003-8125

Ji Hong Kim

Hanyang University

Yeongjun Yoon

Hanyang University https://orcid.org/0000-0001-6122-9632

Sung Gyu Shin

Soongsil University

Won Hyuk Choi

Hanyang University

Jong Hwi Kim

Hanyang University

Yoseph Park

Hanyang University

Joo Sung Kim

RIKEN

Hanbin Choi

North Carolina State University https://orcid.org/0009-0008-7561-1128

Hyo Jeong Kim

Hanyang University https://orcid.org/0009-0005-5680-6235

So Young Kim

Hanyang University

Youngho Eom

Hanyang University https://orcid.org/0000-0002-0922-1155

Jae Hyun Jeong

Soongsil University

Kyeounghak Kim

Hanyang University https://orcid.org/0000-0003-1297-6038

Article

Keywords:

Posted Date: November 17th, 2026

DOI: https://doi.org/10.21203/rs.3.rs-11263263/v1

License: This work is licensed under a Creative Commons Attribution 4.0 International License.
Read Full License

Additional Declarations: There is **NO** Competing Interest.

Reaction-driven ionic remodeling enables durable soft electronics

Ji Hong Kim[1]†, Yeongjun Yoon[1]†, Sung Gyu Shin[2]†, Won Hyuk Choi[1], Jong Hwi Kim[1], Yoseph Park[1], Joo Sung Kim[5], Hanbin Choi[6], Hyo Jeong Kim[7], So Young Kim[1], Youngho Eom[7], Jae Hyun Jeong[2*], Kyeounghak Kim[1*], and Do Hwan Kim[1,3,4*]

[1]*Department of Chemical Engineering, Hanyang University, Seoul 04763, Republic of Korea.*
[2]*Department of Chemical Engineering, Soongsil University, Seoul, 06978, Republic of Korea.*
[3]*Institute of Nano Science and Technology, Hanyang University, Seoul 04763, Republic of Korea.*
[4]*Clean-Energy Research Institute, Hanyang University, Seoul 04763, Republic of Korea.*
[5]*Thin-Film Device Laboratory, RIKEN, 2-1 Hirosawa, Wako, Saitama 351-0198, Japan.*
[6]*Department of Chemical and Biomolecular Engineering, North Carolina State University, Raleigh, NC, USA*
[7]*Department of Organic and Nano Engineering, Human-Tech Convergence Program, Hanyang University, Seoul 04763, Republic of Korea.*

†These authors contributed equally to this work.

*Corresponding authors' email: nfejjh@ssu.ac.kr (J.H.J.), chemekim@hanyang.ac.kr (K.K.), dhkim76@hanyang.ac.kr (D.H.K.)

Abstract

Soft ionic conductors form critical ion-electron interfaces in biointegrated electronics, iontronic sensors and electrochemical transistors, but water and ion loss can cause signal drift, unstable gating and shortened device lifetimes. Here we report a reaction-regulated conductor in which decarboxylation remodels anionic charge carriers while stabilizing the ionic state responsible for ion-electron transduction. In a choline malate-gelatin matrix, water promotes ion dissociation, whereas nucleophilic sites in gelatin convert malate into smaller, more mobile ionic species and reorganize ion-water-polymer interactions. The resulting REACT gel reaches 31.6 mS cm^{-1} and retains over 90% of its conductivity for two years under ambient conditions. Integrated into piezocapacitive pressure sensors and PEDOT:PSS organic electrochemical transistors, REACT provides stable sensing, ionic gating and reproducible switching for seven days, while maintaining cytocompatibility and accelerating wound regeneration in engineered skin organoids. Reaction-driven ionic remodeling thus couples fast ion transport with durable ion-electron transduction across soft electronic and bioelectronic interfaces.

Main

Soft ionic conductors are central to bio-integrated electronics[1-4] and soft wearable systems[5-7], where they form mechanically compliant interfaces for ionic signal transmission and ion-electron transduction. Their long-term operation, however, is often compromised by the gradual loss of water and mobile ions from hydrated materials, leading to changes in ionic transport, signal drift and unstable device operation. Water provides strong dielectric screening[8-10], promotes ion dissociation and increases the population of mobile charge carriers, but its volatility can drive dehydration, ion leakage and performance degradation. Non-volatile ionic liquids and deep eutectic solvents suppress solvent evaporation, yet their lower-dielectric environments can strengthen ion-ion correlations and promote cluster formation[11-13], reducing ionicity and slowing ion transport[14-16]. Existing approaches therefore largely improve ionic stability by regulating the solvation, association or confinement of predefined ionic species, creating an inherent tension between fast ion transport and long-term retention while leaving the chemical identity of the charge carriers unchanged.

Solvation engineering can weaken ion pairing and enhance ion mobility[17-19], but the ionic species themselves are generally fixed during material formulation. We therefore asked whether the charge carriers could instead be chemically transformed within the conductor, such that fast ion transport and long-term ionic stability emerge from the same molecular process. This approach would introduce chemical identity as an additional design variable for ionic transport, enabling the population, size and mobility of charge carriers to be altered *in situ* while simultaneously reorganizing their interactions with water and the polymer matrix. More broadly, such reaction-regulated ionic states could provide a route to stable ion-electron interfaces in soft electronic systems, where both high ionic mobility and persistent material integrity are required for reliable operation.

Here, we realize this concept in REACT (Reaction-Enabled Anion Conversion and Transport), a hydrated choline malate-gelatin conductor in which the matrix chemically remodels anionic charge carriers through decarboxylation (Fig. 1a, Supplementary Fig. 1 and 2). Inspired by biological decarboxylation pathways[20], nucleophilic amine-containing sites in gelatin drive the *in situ* conversion of malate into smaller, more mobile ionic species. This reaction increases the population and diffusivity of mobile ions while reorganizing ion-water-

polymer interactions (Fig. 1b). Unlike conventional approaches that regulate pre-existing ions through solvation or confinement, decarboxylation changes the chemical species that carry charge (Fig. 1c). The resulting REACT gel reaches an ionic conductivity of 31.6 mS cm^{-1} while suppressing water activity, dehydration and ion leakage, and retains more than 90% of its initial conductivity for two years under ambient conditions (Fig. 1d and Table S1). These results establish reaction-driven ionic remodeling as a materials strategy that couples fast ion transport with persistent ionic stability, providing durable ion-electron interfaces for soft electronic and bioelectronic systems.

Matrix-amplified ion dissociation in REACT gels

To determine whether water promotes ion dissociation in hydrophilic ionic liquids, and whether this dissociation pathway can be preserved in the solid electrolyte state, we first quantified ionicity in both liquid and gel systems. We selected three choline-based ionic liquids bearing anions of different kosmotropic strength, malate, glycolate and propionate (Fig. 2a). Among the neat liquids, choline malate (CM) showed the lowest conductivity, consistent with the high charge density of malate and strong cation-anion association. Adding water raised CM conductivity by more than three orders of magnitude, far exceeding the other systems and indicating exceptionally efficient water-induced dissociation of the strongly kosmotropic malate (Supplementary Fig.3).

Because conductivity in liquid electrolytes reflects both free-ion concentration and ion mobility, conductivity alone cannot directly quantify ion dissociation. We therefore constructed Walden plots[21], which decouple conductivity from viscosity-governed mobility and provide a comparative measure of ionicity (Fig. 2b). All neat liquids deviated substantially from the ideal Walden line ($y = x$) and all shifted toward it after hydration. After water addition, their positions shifted toward the ideal line, confirming enhanced ionicity across all systems. Notably, CM showed the lowest ionicity in the neat state but the highest ionicity after hydration, demonstrating that the strong kosmotropic character of malate enables water to most effectively disrupt ion pairing and generate free charge carriers[22-25].

To determine whether the dissociation behavior observed in hydrated liquid mixtures is retained in the solid electrolyte state, we measured cation and anion self-diffusion coefficients by pulsed-field-gradient NMR (Fig. 2c and Supplementary Fig. 4)[26-28]. Diffusivity increased

stepwise from the neat liquid to the hydrated mixture and further to the REACT gel, showing that water-assisted dissociation is not lost upon gelation but amplified within the gelatin matrix. Combining measured conductivity with these diffusivities, we evaluated an apparent ionicity from the inverse Haven ratio[29-31], which quantifies how effectively clustered ions are converted into mobile carriers (see supplementary text for a detailed discussion). Hydration raised the ionicity of CM relative to the neat liquid, whereas the gelatin based REACT gels showed a much larger increase that grew more pronounced at higher ionic liquid loadings (Fig. 2d and Supplementary Fig. 5). This stepwise increase in diffusivity from the neat ionic liquid to the hydrated mixture and finally to the solid gel indicates that water-assisted dissociation is not lost upon gelation but is amplified within the reaction-regulated gelatin matrix. The gelatin framework therefore does not merely contain a hydrated ionic liquid but actively amplifies ion dissociation, forming stable solid networks at ionic liquid contents up to 80 wt% without observable leakage and reaching a maximum ionic conductivity of 31.6 mS cm^{-1} (Fig. 2e and Supplementary Fig. 6).

To elucidate the atomistic origin of the enhanced ionicity and diffusivity, we developed a machine-learning interatomic potential (MLIP) with *ab initio*-level accuracy and performed molecular dynamics (MD) simulations under NVT conditions. Three representative systems were constructed: a neat ionic liquid, a hydrated ionic liquid, and a collagen-containing hydrated ionic liquid that mimics the gelatin-based REACT environment (Supplementary Fig. 7 and Supplementary methods). A detailed description of the experimental procedures is provided in the Computational Details section of Supplementary text. For each system, NVT simulations were performed for 2 ns with 0.5 fs timestep, and stable equilibration of the total energy and temperature was confirmed before structural analysis (Supplementary Fig. 10a-c). We first examined the microscopic organization of ions and water molecules using radial distribution function (RDF) analysis, which describes the probability of finding neighboring species at defined distances from a reference ion (Supplementary Fig. 11).

In the neat ionic liquid, $[Ch]^+$-$[Ma]^{2-}$ correlation appeared at 3.18 Å (Fig. 2f). Upon hydration, this distance increased to 3.68 Å (Fig. 2g), consistent with weakened ion pairing. In the collagen-containing hydrated system, the $[Ch]^+$-$[Ma]^{2-}$ distance remained larger than that in the neat ionic liquid, appearing at 3.33 Å (Fig. 2h). In addition, the $[Ch]^+$-H_2O and $[Ma]^{2-}$-H_2O correlations occurred at shorter distances than the $[Ch]^+$-$[Ma]^{2-}$ ion-pair correlation,

indicating that water preferentially interacts with both ionic species and disrupts direct cation-anion association (Fig. 2g-h). Consistent with this structural reorganization, the diffusion coefficients of both $[Ch]^+$ and $[Ma]^{2-}$ extracted from the MD trajectories increased markedly upon hydration and were further enhanced in the collagen-containing system (Table. S2). These simulations provide atomistic evidence that water and the gelatin-derived matrix cooperatively weaken ion pairing, promote ion dissociation and enhance ion mobility, thereby explaining the experimentally observed increase in ionicity and conductivity in REACT gels (Fig. 2c-e).

Reaction-driven ionic remodeling enhances ion transport

Although hydration enhanced ion dissociation, incorporation of the gelatin-derived matrix produced a substantially larger increase in apparent ionicity. MD trajectories revealed progressive fragmentation of $[Ma]^{2-}$ into smaller C_4, C_2, and C_1 species, which was most extensive in the collagen-containing system, together with deprotonation of gelatin-derived residues (Table S3). These observations suggest that nucleophilic sites in the gelatin matrix promote amine-assisted malate decarboxylation (Fig. 3a)[32,33], increasing the number of mobile charge carriers while reducing their effective size. This mechanism resembles biologically mediated decarboxylation pathways in which local nucleophilic and proton-transfer environments facilitate C-C bond cleavage[34], supporting a reaction-regulated ionic remodeling mechanism rather than simple ion-pair dissociation.

We experimentally tested this mechanism by monitoring electrolyte pH and CO_2 evolution. The pH progressively decreased from neat CM to hydrated CM and further upon gelatin incorporation (Fig. 3b), consistent with CO_2 formation from malate decarboxylation[35,36]. Because MD identified CO_2 as a C_1 product of $[Ma]^{2-}$ decomposition (Table S2), real-time gas chromatography was performed and detected a distinct CO_2 signal only in the gelatin-containing system (Fig. 3c), directly supporting matrix-assisted decarboxylation. Finally, adding proline to chitosan ion gels markedly increased ionic conductivity and produced an approximately threefold increase in apparent ionicity (Supplementary Fig. 12), indicating that amine-assisted anion remodeling can extend beyond gelatin to other polymer matrices.

Finally, we visualized ion transport by mapping the diffusion trajectories of choline nitrogen ($N[Ch]^+$) and malate carboxyl carbon ($C[COO]^-$) across the simulated systems. In the pure IL (Fig. 3d), ions remained highly localized within tight coordination shells, indicating severe spatial confinement. Hydration (Fig. 3e) weakened ionic association through water-

mediated solvation, allowing broader diffusion. Most notably, the collagen-incorporated system (Fig. 3f) exhibited an extensively expanded diffusion network. Beyond hydration, this enhancement originates from the ion avalanche effect, in which $[Ma]^{2-}$ fragmentation into lower-molecular-weight C_1-C_4 species reduces kinematic resistance and generates highly mobile fragments. Consequently, these highly mobile fragments generate an extensive and interconnected web of diffusion paths, underpinning the system's superior transport properties.

Ion-polymer-water networks stabilize REACT gels

To identify the molecular origin of REACT gel stability, we examined interactions among CM, water, and gelatin using XPS and FT-IR. XPS revealed a quaternary ammonium N^+R_3 signal after CM incorporation (Fig. 4a and Supplementary Fig. 13), which shifted from 400.86 to 401.06 eV as CM content increased from 50 to 80 wt%. Concurrent positive shifts in C-N- and amide-related signals indicate reduced local electron density and strengthened electrostatic and hydrogen-bonding interactions between choline and gelatin[37]. FT-IR further showed an O-H red shift from 3312 to 3242 cm^{-1} and a C=O shift from 1640 to 1657 cm^{-1} (Supplementary Fig. 14), corroborating strong ion-polymer-water coupling. Together, these results indicate that a dense interaction network immobilizes ionic species and lowers water activity, enabling REACT gels to suppress ion leakage and solvent loss through matrix-mediated interactions rather than simple physical entrapment.

To determine whether these interactions produce atomistic structural organization, we performed MD simulations using a dual-collagen model representing the gelatin-derived scaffold (Supplementary Fig. 9d). Because the cationic nitrogen of choline ($N[Ch]^+$) can interact electrostatically with electron-rich oxygen atoms in collagen, we analyzed $[Ch]^+$ mobility as a function of distance from the collagen interface. $[Ch]^+$ diffusion was strongly suppressed near the collagen surface, with the most immobilized ions localized in interstitial voids between adjacent helices (Fig. 4b and Supplementary Fig. 15). Structural and trajectory analyses further confirmed persistent confinement within these sites (Supplementary Fig. Supplementary Fig. 16 and Supplementary video1), indicating that trapped $[Ch]^+$ ions act as electrostatic bridges between neighboring collagen molecules. In contrast, $[Ma]^{2-}$ showed broad spatial distributions with little dependence on collagen proximity (Supplementary Fig. 17), suggesting weak interfacial anchoring and a smaller contribution to physical cross-linking.

Consistent with the MD results, these ion-polymer interactions stabilized the gelatin scaffold at the macroscopic level. Gelatin hydrogels exhibit a characteristic low-angle X-ray diffraction peak at approximately $2\theta = 6°$, associated with triple-helical domains formed through water-mediated interactions[38]. This peak increased with ionic liquid content (Fig. 4c), indicating progressive stabilization of ordered gelatin domains. The reinforcement was accompanied by increased elasticity and toughness (Supplementary Fig. 18), while frequency-dependent rheology showed a shift of the gel-point frequency to higher values (Supplementary Fig. 19), consistent with a strengthened internal network and enhanced dynamic bonding.

The thermal stabilization of the gelatin matrix was further examined by differential scanning calorimetry (DSC) (Fig. 4d). Increasing ionic liquid content markedly increased the denaturation enthalpy of gelatin, indicating enhanced preservation of the triple-helical structure against thermal disruption (Supplementary Fig. 20). Notably, no water-freezing transition was observed down to -50 °C, suggesting strong coordination of water within the ionic liquid-gelatin network. This bound-water state suppresses ice crystallization and provides a thermodynamic basis for solvent retention in REACT gels.

To assess water activity and its response to ambient humidity, we performed dynamic vapor sorption (DVS) over a full adsorption-desorption cycle (Fig. 4e)[39]. The conventional hydrogel exhibited a mass change exceeding 342 wt% and pronounced hysteresis of 28%, consistent with strong osmotic water uptake by freely mobile ions under humidity[40,41]. In contrast, the REACT gel showed less than half the mass change and nearly negligible hysteresis (0.03%), indicating highly reversible water exchange within well-defined binding environments. This behavior is attributed to the dense electrostatic and hydrogen-bonding network among choline, remodeled malate species, water, and gelatin, which reduces the thermodynamic activity of water. Accordingly, water activity ($\alpha\omega$) remained consistently lower in the REACT gel (Supplementary Fig. 21)[42], supporting suppressed evaporation even under low humidity.

We further probed the microscopic mobility of water in the gel network using ^{1}H NMR transverse relaxation time (T_2) measurements (Fig. 4f)[43-45]. T_2 reflects the rotational and translational mobility of water molecules, with shorter relaxation times indicating stronger confinement. As the CM content increased, the T_2 values decreased markedly, showing that

water motion becomes increasingly restricted through interactions with the ionic species and the gelatin scaffold. Whereas DVS analysis establishes the reduced water activity from a thermodynamic perspective, the shortened T_2 relaxation provides dynamic evidence that water is converted from a relatively mobile state into a more strongly bound state within the REACT gel. Together, these results explain the enhanced dehydration resistance of REACT gels. Despite its lower initial water fraction, the REACT gel retained the highest water content after two weeks (Supplementary Fig. 22). SEM further revealed a dense, nearly pore-free morphology compared with the porous structure of lower-CM gels (Supplementary Fig. 23), consistent with a compact network that suppresses water loss.

We next evaluated the electrochemical performance of REACT gels for device integration. Under the same 0.5 V bias, the REACT gel exhibited a substantially higher current density than a chitosan-based ion gel, while requiring more than threefold lower voltage to sustain the same current (Supplementary Fig. 24). It also maintained a stable current density of 27 mA cm^{-2} under a 10 Hz pulsed DC bias, demonstrating high-current ionic operation under dynamic stimulation (Supplementary Fig. 25). We then examined ion leakage and electrochemical stability under physiologically relevant aqueous conditions. Conventional ionic hydrogels gradually lose mobile ions to the surrounding medium, leading to decreased ionic conductivity (Supplementary Fig. 26a). In contrast, the dense gelatin-CM-water interaction network in the REACT gel suppresses ion efflux, while PBS ions permeate into the gel and increase its ionic conductivity (Supplementary Fig. 26 b,c). Consistently, FT-IR spectra of PBS after one day of immersion showed no detectable CM-derived peaks, confirming negligible ionic-liquid leakage (Supplementary Fig. 26d). Long-term electrochemical durability was further evaluated during one month of PBS immersion. Free-ion density and ion mobility were tracked by frequency-dependent dielectric analysis using the relaxation behavior of tan δ ($\varepsilon''/\varepsilon'$), whose peak frequency reflects changes in ion population and transport dynamics[46]. Ion and water influx caused an initial change during the first 24 h, after which the free-ion density reached a steady state and remained stable for nearly one month (Supplementary Fig. 27). Finally, cyclic voltammetry showed no observable redox activity within ±2 V despite the presence of water (Supplementary Fig. 28). This stability is attributed to the strongly coupled CM-water-gelatin network, which restricts water and ionic species and suppresses parasitic electrochemical reactions.

Reaction-regulated ion transport enables stable ion-electron transduction

Having established the reaction-regulated origin of high ionicity, dehydration resistance and ion-retention in REACT gels, we next examined whether this ionic state could be translated into functional soft devices. Soft ionic conductors are attractive materials for bioelectronic interfaces[47,48], ionic sensors[49,50] and ion-coupled transistors[51,52] because mobile ions can mediate charge transport, interfacial coupling and stimulus-responsive electrical outputs in soft, hydrated systems. However, practical device operation is often limited by water evaporation, ion leakage, mechanical relaxation and unstable ionic gating. The high free-ion density, suppressed ion efflux, stable hydration state and low-voltage current generation of REACT gels therefore provide a general materials platform for stable ion-mediated devices.

We first evaluated the REACT gel as a bioelectronic interface for electrically assisted wound regeneration. Because wound repair in animal models can be influenced by immune responses, systemic regulation and inter-individual variability, an engineered skin organoid model was used to isolate the material-specific contribution of stable ionic stimulation (Fig. 5a). Before stimulation experiments, cytocompatibility was assessed using Transwell-based MTT assays with human dermal fibroblasts and keratinocytes (Supplementary Fig. 29a). NaCl-containing PEO-based hydrogels showed pronounced cytotoxicity, with cell viability decreasing below 40% after 48 h (Supplementary Fig. 29b), likely owing to salt diffusion into the culture medium. Chitosan-based ion gels improved cell viability but still showed partial metabolic suppression. By contrast, REACT gels maintained high cell viability of more than 80% after 48 h across the tested ionic liquid loadings, indicating that the gelatin matrix effectively stabilizes ionic components while preserving cytocompatibility (Supplementary Fig. 29c).

The effect of REACT-mediated ionic stimulation on wound regeneration was then examined by separately analyzing horizontal wound closure and vertical epidermal reconstruction (Supplementary Fig. 30 and 31). In the organoid wound model, epidermal keratinocytes migrated toward the wound center and progressively repopulated the damaged region. REACT gel stimulation markedly accelerated wound closure relative to the untreated control (Fig. 5b). The time required to reach 80% wound closure decreased from 48 h in the control group to 21 h with REACT gel stimulation, corresponding to a 56% acceleration

(Supplementary Fig. 32). Optical coherence tomography further enabled non-destructive cross-sectional analysis of epidermal regeneration after CO_2 laser-induced micro-wounding (Supplementary Fig. 33). Epidermal reconstruction proceeded through basal layer recovery, upper-layer differentiation and eventual keratinization[53]. Under REACT gel stimulation, the time required to reach 80% epidermal regeneration decreased from 167 h to 96 h, representing a 43% improvement in regeneration rate (Fig. 5c). These findings demonstrate that stable ionic stimulation from the REACT gel enhances both epithelial migration and stratified epidermal reconstruction.

Biochemical analyses further showed that REACT gel stimulation promotes functional tissue remodeling (Fig. 5d). Pro-collagen production, a marker of dermal extracellular matrix formation, increased from 332 ng in the control group to 456 ng in the REACT gel-treated group. Secretion of vascular endothelial growth factor also increased by 15-25% relative to the control. To assess whether these secreted factors enhanced angiogenic activity, conditioned media from the wound models were applied to human umbilical vein endothelial cells. Tubule formation assays revealed substantially enhanced angiogenic network formation after REACT gel stimulation: the number of vascular segments increased from 18 to 35, while junction and mesh numbers increased by 62% and 187%, respectively (Supplementary Fig. 34). Thus, REACT-mediated ionic stimulation accelerates not only morphological wound closure, but also extracellular matrix remodeling and angiogenic signaling in engineered skin tissue.

We next assessed whether the stable ionic state of REACT gels could improve soft pressure sensing. Piezocapacitive type (showing metal-dielectric-metal) sensors were fabricated using a PEO hydrogel, a chitosan ion gel or a REACT gel as the dielectric layer, and their pressure response was compared over time. The PEO hydrogel sensor showed a progressive decrease in baseline capacitance from day 1 to day 7, together with pronounced stress relaxation, consistent with water evaporation and mechanical instability in the water-rich matrix (Extended Data Figs. 1a and 2). The chitosan ion gel sensor showed a reduced capacitance response after one day, suggesting pressure-induced ion loss before reaching a more stable state (Extended Data Fig. 1b). In contrast, the REACT gel sensor maintained nearly unchanged capacitance responses over seven days under repeated pressure loading (Extended Data Fig. 1c). Among the three materials, only the REACT gel enabled stable pressure-dependent capacitance modulation with low variation in switching time and sensitivity over

time, demonstrating that its ion-retentive and mechanically stabilized network supports reliable ionic sensing (Extended Data Fig. 1d-f).

Finally, we integrated REACT gels into organic electrochemical transistors (OECTs), in which efficient ionic gating is required to couple ion transport in the electrolyte with electronic transport in the organic mixed ionic-electronic conductor channel. Poly(3,4-ethylenedioxythiophene)-poly(styrenesulfonate) (PEDOT:PSS) based OECTs were fabricated using each soft ionic conductor as the electrolyte. Hydrogel-based OECTs showed gradual shifts in transfer characteristics over seven days, with reliable transistor operation lost after three days, consistent with dehydration, ion precipitation and perturbation of the electrolyte-channel interface (Extended Data Fig. 2a)[54,55]. Chitosan ion gel-based OECTs showed negligible transistor modulation, reflecting limited ion transport and strong ion clustering that suppresses ion penetration into the PEDOT:PSS channel (Extended Data Fig. 2b). By contrast, REACT gel-based OECTs maintained stable transfer characteristics with minimal variation over seven days (Extended Data Fig. 2c). The REACT gel also produced the fastest and most stable switching response among the tested devices, confirming efficient and reproducible ionic gating of the PEDOT:PSS channel (Extended Data Fig. 2d-i).

Together, these demonstrations establish REACT gels as stable soft ionic conductors that translate reaction-regulated ion remodeling into device-level function. Across bioelectronic wound stimulation, pressure sensing and OECT gating, the same materials principle, high free-ion density combined with suppressed water loss and ion leakage, enables stable ion transport, interfacial coupling and ion-to-electron transduction in soft device environments.

Discussion

In conclusion, we establish a reaction-regulated hydrated ionic conductor in which decarboxylation chemically remodels the charge carriers. Unlike conventional soft ionic conductors that regulate the solvation, association or mobility of pre-existing ions, REACT transforms the ionic species themselves, increasing both the population and diffusivity of mobile charge carriers. This carrier remodeling is coupled to a reorganized ion-water-polymer network that suppresses water loss and ion leakage while sustaining high ionic conductivity and long-term ionic stability. Transport and retention therefore arise from the same reaction-regulated ionic state rather than from independent optimization of conductivity and stability.

This stabilized ionic state translates directly into persistent electronic function, supporting reliable pressure sensing, stable OECT gating and reproducible ion-electron transduction.

More broadly, these results establish chemical transformation of charge carriers as a design principle for soft electronic interfaces. By coupling *in situ* anion remodeling with stabilization of the surrounding hydrated matrix, REACT connects molecular ion chemistry to device-level reliability across bioelectronic interfaces, ionic sensors and OECT-based transducers. Ion transport in soft electronics can therefore be programmed not only by controlling the environment through which ions move, but also by changing which ionic species carry charge. Reaction-driven ionic remodeling thus provides an additional degree of freedom for engineering soft ionic conductors in which fast transport, material retention and stable ion-electron transduction are intrinsically coupled, offering a route towards durable soft electronic and bioelectronic systems.

Methods

Synthesis of choline-malate $[Ch]^+[MA]^-$ ionic liquid

Choline-Malate ($[Ch]^+[MA]^-$) ionic liquid was synthesized via salt metathesis. A 2 M solution of malic acid in methanol was gradually introduced to a 0.8 M solution of choline bicarbonate (Sigma-Aldrich; St. Louis, MO, USA) under gentle stirring at 25 °C for 4 hours to allow the release of carbon dioxide. Methanol and water were removed through rotary evaporation at 80 °C for 12 hours, followed by drying in a vacuum oven at 80 °C for 48 hours.

Soft ionic conductor fabrication (hydrogel, ion gel, and REACT gel)

A PEO-based hydrogel was prepared by photo-crosslinking a precursor solution composed of poly(ethylene oxide) (PEO), poly(ethylene glycol) dimethacrylate (PEGDMA) as a crosslinker, a photoinitiator, and sodium chloride (NaCl) as the ionic source. First, 1 g of PEO (40wt%) was dissolved in 1.5 g of deionized water, and the mixture was stirred until a homogeneous and transparent solution was obtained. PEGDMA was then added at 10 wt% relative to PEO (0.1 g), followed by 0.0016 g of the photoinitiator. NaCl was incorporated at a final concentration of 3 M (0.263 g) to provide the mobile ionic species. The complete precursor solution was stirred until fully homogeneous and degassed to remove trapped air bubbles. The solution was subsequently cast into a mold or onto a substrate and exposed to UV irradiation to induce crosslinking of the PEGDMA network, yielding the PEO-based ion gel film. The cured film

was peeled from the substrate to obtain a free-standing hydrogel.

To formulate the ion gel solution, a chitosan was first prepared by dissolving medium molecular weight chitosan (Sigma-Aldrich, Saint Louis, MO, USA) at 2 wt% in an aqueous acetic acid solution (1 v/v%, 99.7%, DAEJUNG, Korea). The 50wt% of synthesized CM was then introduced into this chitosan solution. The mixture was stirred at room temperature for 24 hours, after which it was sonicated for 30 minutes to ensure uniform dispersion of the ionic liquid throughout the solution.

REACT gel was formulated using a combination of choline-derived ionic liquids (ILs), water and gelatin biopolymers. CM ILs were integrated into a gelatin solution containing 10 wt% bovine skin gelatin (gel strength ~225 g Bloom, Sigma-Aldrich, G9382) dissolved in deionized water. Varying concentrations of CM ILs (0, 10, 30, 50, 70, 80 wt%) were thoroughly blended with the gelatin solution and allowed to react for 24 hours at 60 ℃, a temperature surpassing the gelatin sol-gel transition point. Subsequently, 3 g of the gelatin $[Ch]^+[MA]^-$ solution was cast into a glass petri dish and cured for 48 hours at room temperature. The resulting film was carefully peeled off the substrate, yielding the REACT film.

Fabrication of iontronic devices

Piezocapacitive sensor devices were fabricated by sandwiching the Soft ionic conductor films (film thickness ~ 500 μm, film area 0.75 cm^2) between two Au electrodes (surface resistance ~ 10 Ω sq^{-1}). The gold wires (Nilaco Corp., diameter: 50 μm) were attached to the electrodes for connections with the measuring instrument. To fabricate soft ionic conductor based organic electrochemical transistor (OECT), a heavily *n*-doped Si/SiO_2 wafer (SiO_2 thickness: 3000 Å) was used as a substrate to fabricate the devices. The Si substrate was cleaned with acetone, isopropyl alcohol (IPA), and DI water, followed by O2 plasma treatment (100 W, 100 s). Subsequently, Source/Drain electrodes of the OECT were thermally evaporated onto the substrate through a patterned shadow mask under a pressure of 8.0×10^{-6} torr (VTR 5006, SNTEK). Then, the PEDOT:PSS dispersion was spin-coated on the substrate with patterned electrodes and annealed at 150 °C for 1 hour. The gate and channel areas of PEDOT:PSS were covered by patterned PDMS masks, and the samples were dry etched (O2 75 sccm, CH4 25 sccm, 150 W, 30 s) to define each terminal. Subsequently, the prepared REACT gel was cast onto the deposited PEDOT:PSS channel areas. Finally, Cr/AU deposited electrode is integrated onto the REACT gel.

Computational Details

To investigate the atomistic mechanisms of ion dissociation and transport within the gel matrix, we performed density functional theory (DFT) calculations and machine-learning interatomic potential (MLIP)-based molecular dynamics (MD) simulations. Training datasets for the pure ionic liquid, hydrated ionic liquid, and collagen-containing systems were generated via on-the-fly machine learning force field (MLFF) calculations using Vienna Ab-initio Simulation Package (VASP, version 6.4.3)[56,57]. An MLIP was subsequently trained using the SevenNet[58] framework to accurately describe the complex potential energy surfaces of these systems. Based on this potential, production MD simulations were conducted using Large-scale Atomic/Molecular Massively Parallel Simulator (LAMMPS)[59] under NVT conditions for 2 ns to analyze radial distribution functions, ion diffusion trajectories, and interfacial dynamics. Detailed descriptions of the computational models, DFT functional parameters, MLIP training protocols, and specific MD simulation settings are provided in the Computational Details section of the Supplementary Information.

References

1 Li, Na, et al. Rapid self-assembly of robust ultrathin ionogel films for high-performance bioelectronics. *Sci. Adv.* **12,** eaeb4391 (2026).

2 Li, Leqi, et al. Paintable, fast gelation, highly adhesive hydrogels for high-fidelity electrophysiological monitoring wirelessly. *Small* **21,** 2407996 (2025).

3 Wang, Chunya, et al. On-skin paintable biogel for long-term high-fidelity electroencephalogram recording. *Sci. Adv.* **8,** eabo1396 (2022).

4 Jo, Young Jin, et al. Biocompatible and biodegradable organic transistors using a solid-state electrolyte incorporated with choline-based ionic liquid and polysaccharide. *Adv. Funct. Mater.* **30,** 1909707 (2020).

5 Lee, Hyunjae, et al. Ultrathin organic electrochemical transistor with nonvolatile and thin gel electrolyte for long-term electrophysiological monitoring. *Adv. Funct. Mater.* **29,** 1906982 (2019).

6 Wang, Weiguang, et al. Cholinium-based eutectogel electrode for high-quality dynamic EEG/ECG monitoring exceeding 48 hours. *npj Flex. Electron.* **9,** 121 (2025).

7 Zhang, Zongman, et al. A 10-micrometer-thick nanomesh-reinforced gas-permeable hydrogel skin sensor for long-term electrophysiological monitoring. *Sci. Adv.* **10,** eadj5389 (2024).

8 Pan, Liang, et al. A compliant ionic adhesive electrode with ultralow bioelectronic impedance. *Adv. Mater.* **32,** 2003723 (2020).

9 Yang, Jianbo, et al. Antifreezing zwitterionic hydrogel electrolyte with high conductivity of 12.6 mS cm− 1 at− 40° C through hydrated lithium ion hopping migration. *Adv. Funct. Mater.* **31,** 2009438 (2021).

10 Park, Jae Hyun, et al. Water-assisted increase of ionic conductivity of lithium poly (acrylic acid)-based aqueous polymer electrolyte. *ACS Appl. Energy Mater.* **3,** 10119-10130 (2020).

11 Peng, Xu, et al. A zwitterionic gel electrolyte for efficient solid-state supercapacitors. *Nat. commun.***7,** 11782 (2016).

12 Judeinstein, Patrick, et al. Structural and dynamical heterogeneities at the nanoscale in alkali/earth alkaline ionic liquid electrolytes: experiment and molecular simulation. *Phys. Chem. Chem. Phys.* **28,** 3850-3865 (2026).

13 Shankar, Samanvitha Kunigal Vijaya, et al. Impact of Li, Na and Zn metal cation concentration in EMIM–TFSI ionic liquids on ion clustering, structure and dynamics. *Phys. Chem. Chem. Phys.* **26,** 7049-7059 (2024).

14 Gouverneur, Martin, et al. Direct determination of ionic transference numbers in ionic liquids by electrophoretic NMR. *Phys. Chem. Chem. Phys.* **17,** 30680-30686 (2015).

15 Warrington, Anna, et al. Investigation of properties and performance of three novel highly concentrated ether-functionalised ionic liquid electrolytes for lithium metal batteries. *Energy Storage Mater.* **63,** 102984 (2023).

16 Mariani, Alessandro, et al. The unseen evidence of Reduced Ionicity: The elephant in (the) room temperature ionic liquids. *J. Mol. Liq.* **324,** 115069 (2021).

17 Wang, Yaqing, et al. Ionicity of deep eutectic solvents by Walden plot and pulsed field gradient nuclear magnetic resonance (PFG-NMR). *Phys. Chem. Chem. Phys.* **22,** 25760-25768 (2020).

18 Liu, Xu, et al. Locally concentrated ionic liquid electrolyte with partially solvating diluent for lithium/sulfurized polyacrylonitrile batteries. *Adv. Mater.* **34,** 2207155 (2022).

19 Wang, Zhicheng, et al. Intrinsically nonflammable ionic liquid-based localized highly concentrated electrolytes enable high-performance Li-metal batteries. *Adv. Energy Mater.* **11,** 2003752 (2021).

20 Shan, Nan, et al. Cucumber malate decarboxylase, CsNADP-ME2, functions in the balance of carbon and amino acid metabolism in fruit. *Hortic. Res.* **10,** uhad216 (2023).

21 Kobayashi, Y., Tokishita, S. & Yamamoto, H. Determination of Hansen solubility parameters of ionic liquids by using Walden plots. *Ind. Eng. Chem. Res.* **59,** 14217-14223 (2020).

22 Rengstl, D., Fischer, V. & Kunz, W. Low-melting mixtures based on choline ionic liquids. *Phys. Chem. Chem. Phys.* **16,** 22815-22822 (2014).

23 Fang, J. et al. High selectivity framework polymer membranes chemically tuned towards fast anion conduction. *Nat. Commun.* **16,** 3282 (2025).

24 Hong, Yuri, et al. Hydrophobicity of arginine leads to reentrant liquid-liquid phase separation behaviors of arginine-rich proteins. *Nat. commun.* **13,** 7326 (2022).

25 Oh, K.S. et al. Conflicting entropy-driven zwitterionic dry polymer electrolytes for scalable high-energy all-solid-state batteries. *Nat. Commun.* (2025).

26 D'agostino, C. et al. Molecular motion and ion diffusion in choline chloride based deep eutectic solvents studied by 1 H pulsed field gradient NMR spectroscopy. *Phys. Chem. Chem. Phys.* **13,** 21383-21391 (2011).

27 Pagès, Guilhem, et al. Pulsed-field gradient nuclear magnetic resonance measurements (PFG NMR) for diffusion ordered spectroscopy (DOSY) mapping. *Analyst* **142,** 3771-3796 (2017).

28 Guo, Xiaoai, et al. Diffusion in Polymer Solutions: Molecular Weight Distribution by PFG-NMR and Relation to SEC. *Macromol. Chem. Phys.* **218,** 1600440 (2017).

29 Elgharbawy, Amal Ahmed, et al. Implementation of definite screening design in optimization of in situ hydrolysis of EFB in cholinium acetate and locally produced cellulase combined system. *Waste biomass valorization* **8,** 839-850 (2017).

30 Murch, G. E. The haven ratio in fast ionic conductors. *Solid State Ion.* **7,** 177-198 (1982).

31 Nürnberg, P. et al. Superionicity in ionic-liquid-based electrolytes induced by positive ion–ion correlations. *J. Am. Chem. Soc.* **144,** 4657-4666 (2022).

32 Han, J. & Fussenegger, M. Designing supramolecular catalytic systems for mammalian synthetic metabolism. *Nat. Rev. Mater.* **10,** 584-603 (2025).

33 Shoulders, M.D., Raines, R.T. Collagen structure and stability. *Annu. Rev. Biochem.* **78,** 929-958 (2009)

34 Tao, X., Yang, Z., Tong, L. Crystal structures of substrate complexes of malic enzyme and insights into the catalytic mechanism. *Structure* **11,** 1141-1150 (2003)

35 Bera, P.P. et al. Gas and Aqueous Phase Computations on the Keto–Enol Tautomerization of Pyruvic and Zymonic Acids: Implications for Prebiotic Enol Phosphates. *J. Phys. Chem. A.* **129,** 7287-7295 (2025).

34 Edens, W.A. Urbauer, J.L. & Cleland, W.W. Determination of the chemical mechanism of malic enzyme by isotope effects. *Biochemistry* **36,** 1141-1147 (1997)

35 Grahn, E. et al. Control of intracellular pH and bicarbonate by CO2 diffusion into human sperm. *Nat. Commun.* **14,** 5395 (2023).

36 Cano, A. et al. Relevant electronic interactions related to the coordination chemistry of tetracyanometallates. An XPS study. *New J. Chem.* **43,** 18384-18393 (2019).

37 Mosleh, Y. et al. The structure–property correlations in dry gelatin adhesive films. *Adv. Eng. Mater.* **23,** 2000716 (2021).

38 Guo, X., Wu, Y. & Xie, X. Water vapor sorption properties of cellulose nanocrystals

and nanofibers using dynamic vapor sorption apparatus. *Sci Rep.* **7,** 14207 (2017).

39 Díaz-Marín, Carlos D., et al. Physics-based prediction of moisture-capture properties of hydrogels. *Nat. Commun.* **15,** 8948 (2024).

40 Firky, M. et al. Mathematical modeling of sorption isotherms and the thermodynamic properties of vacuum-dried and freeze-dried Barhi dates. *Sci. Rep.* **15,** 19781 (2025).

41 Passauer, L. et al. Dynamic moisture sorption characteristics of xerogels from water-swellable oligo(oxyethylene) lignin derivatives. *ACS Appl. Mater. Interfaces.* **4,** 5852–5862 (2012).

42 McConville, Patrick, and J. M. Pope. 1H NMR T2 relaxation in contact lens hydrogels as a probe of water mobility. *Polymer* **42,** 3559-3568 (2001).

43 Traore, Amidou, Loic Foucat, and Jean-Pierre Renou. 1H-NMR study of water dynamics in hydrated collagen: transverse relaxation-time and diffusion analysis. *Biopolymers* **53,** 476-483 (2000).

44 Hills, B. P., S. F. Takacs, and Peter S. Belton. A new interpretation of proton NMR relaxation time measurements of water in food. *Food Chem.* **37,** 95-111 (1990).

45 Wang, Y. et al. Decoupling of ionic transport from segmental relaxation in polymer electrolytes. *Phys. Rev. Lett.* **108,** 088303 (2012).

46 Yuk, Hyunwoo, Baoyang Lu, and Xuanhe Zhao. Hydrogel bioelectronics. *Chem. Soc. Rev.* **48,** 1642-1667 (2019).

47 Yuk, Hyunwoo, Jingjing Wu, and Xuanhe Zhao. Hydrogel interfaces for merging humans and machines. *Nat. Rev. Mater.* **7,** 935-952 (2022).

48 You, Insang, et al. Artificial multimodal receptors based on ion relaxation dynamics. *Science* **370,** 961-965 (2020).

49 He, Yunfeng, et al. Creep-free polyelectrolyte elastomer for drift-free iontronic sensing. *Nat. Mater.* **23,** 1107-1114 (2024).

50 Torricelli, Fabrizio, et al. Electrolyte-gated transistors for enhanced performance bioelectronics. *Nat. Rev. Methods Primers.* **1,** 66 (2021).

51 Lu, Linlin, et al. Stretchable all-gel organic electrochemical transistors. *Nat. Commun.* **16,** 3831 (2025).

52 Segre, Julia A. Epidermal barrier formation and recovery in skin disorders. *J. Clin. Invest.* **116,** 1150-1158 (2006).

53 Rousselle, Patricia, Fabienne Braye, and Guila Dayan. Re-epithelialization of adult skin wounds: Cellular mechanisms and therapeutic strategies. *Adv. Drug Deliv. Rev.* **146,** 344-365 (2019).

54 Kim, Seong-Min, et al. Influence of PEDOT: PSS crystallinity and composition on electrochemical transistor performance and long-term stability. *Nat. commun.* **9,** 3858 (2018).

55 Lu, Dongdong, and Hu Chen. Solid-state organic electrochesmical transistors (OECTs) based on gel electrolytes for biosensors and bioelectronics. *J. Mater. Chem. A.* **13,** 136-157 (2025).

56 Kresse, G. & Furthmüller, J. Efficiency of ab-initio total energy calculations for metals and semiconductors using a plane-wave basis set. Comput. Mater. Sci. **6**, 15–50 (1996).

57 Kresse, G. & Furthmüller, J. Efficient iterative schemes for ab initio total-energy calculations using a plane-wave basis set. Phys. Rev. B **54**, 11169–11186 (1996).

58 Park, Y. et al. Scalable parallel algorithm for graph neural network interatomic potentials in molecular dynamics simulations. J. Chem. Theory Comput. **20**, 4857–4868 (2024).

59 Thompson, A. P. et al. LAMMPS — a flexible simulation tool for particle-based materials modeling at the atomic, meso, and continuum scales. Comput. Phys. Commun. **271**, 108171 (2022).

Acknowledgments

This work was supported by the National Research Foundation of Korea (NRF) grant funded by the Korea government (MSIT) (RS-2025-00515479, RS-2024-00405818, RS-2024-00358960, RS-2022-NR070840, RS-2026-25494453).

Author contributions

J.H.J., K.K. and D.H.K. supervised the project. D.H.K., J.H.J., K.K., Ji Hong Kim, Y.Y. and S.G.S. developed the theoretical concepts and designed the experiments. Ji Hong Kim carried out all the experiments. Y.Y. and K.K. designed the computational study. Ji Hong Kim and Y.Y. developed the machine-learning interatomic potential, constructed the atomistic model systems, performed all molecular dynamics simulations and analyzed the results, including radial distribution functions, ion diffusion coefficients, decarboxylation pathways and interfacial ion dynamics. K.K. supervised the computational work. W.H.C., Y.P., Jong Hwi Kim, J.S.K., and H.C. helped with experimental procedures. D.H.K., K.K. and J.H.J. reviewed and provided feedback on the manuscript. D.H.K., K.K., J.H.J. Ji Hong Kim, Y.Y. and S.G.S. wrote the manuscript, with D.H.K. responsible for revisions. All authors discussed the results and contributed to the final manuscript.

Competing interests

The authors declare that they have no competing interests.

Data and materials availability

All data are available in the main text or the supplementary materials.

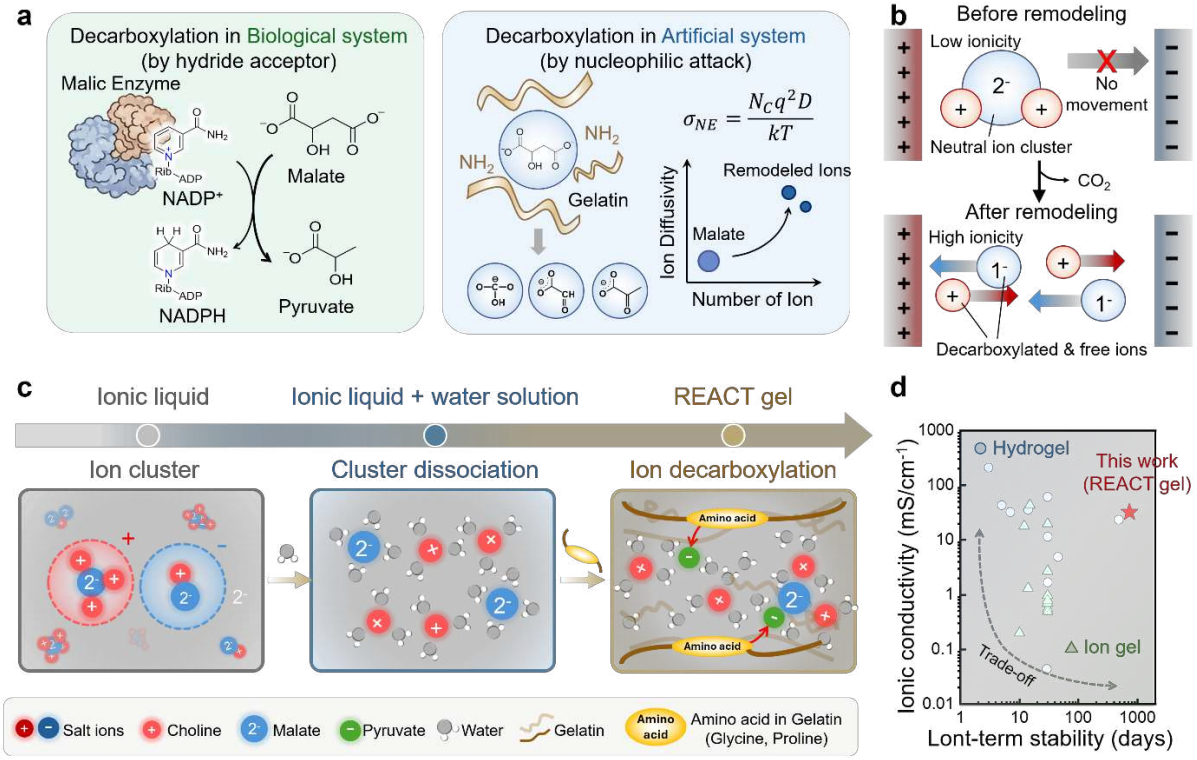


Fig. 1| Reaction-driven ionic remodeling in a durable soft ionic conductor. a, Bioinspired concept of charge-carrier remodeling by decarboxylation. In the REACT system, nucleophilic sites in gelatin promote malate conversion into smaller ionic species, increasing the population and diffusivity of mobile ions. **b,** Schematic comparison of ion transport before and after anion remodeling, illustrating how conversion of divalent malate into smaller ionic species reduces electrostatic constraints on ion motion. **c,** Sequential formation of the REACT ionic state. Hydration first promotes cluster dissociation, followed by gelatin-mediated malate decarboxylation that generates smaller, more mobile ionic species within the hydrated polymer matrix. **d,** Benchmark comparison of ionic conductivity and long-term stability of the REACT gel with previously reported hydrogels and ion gels.

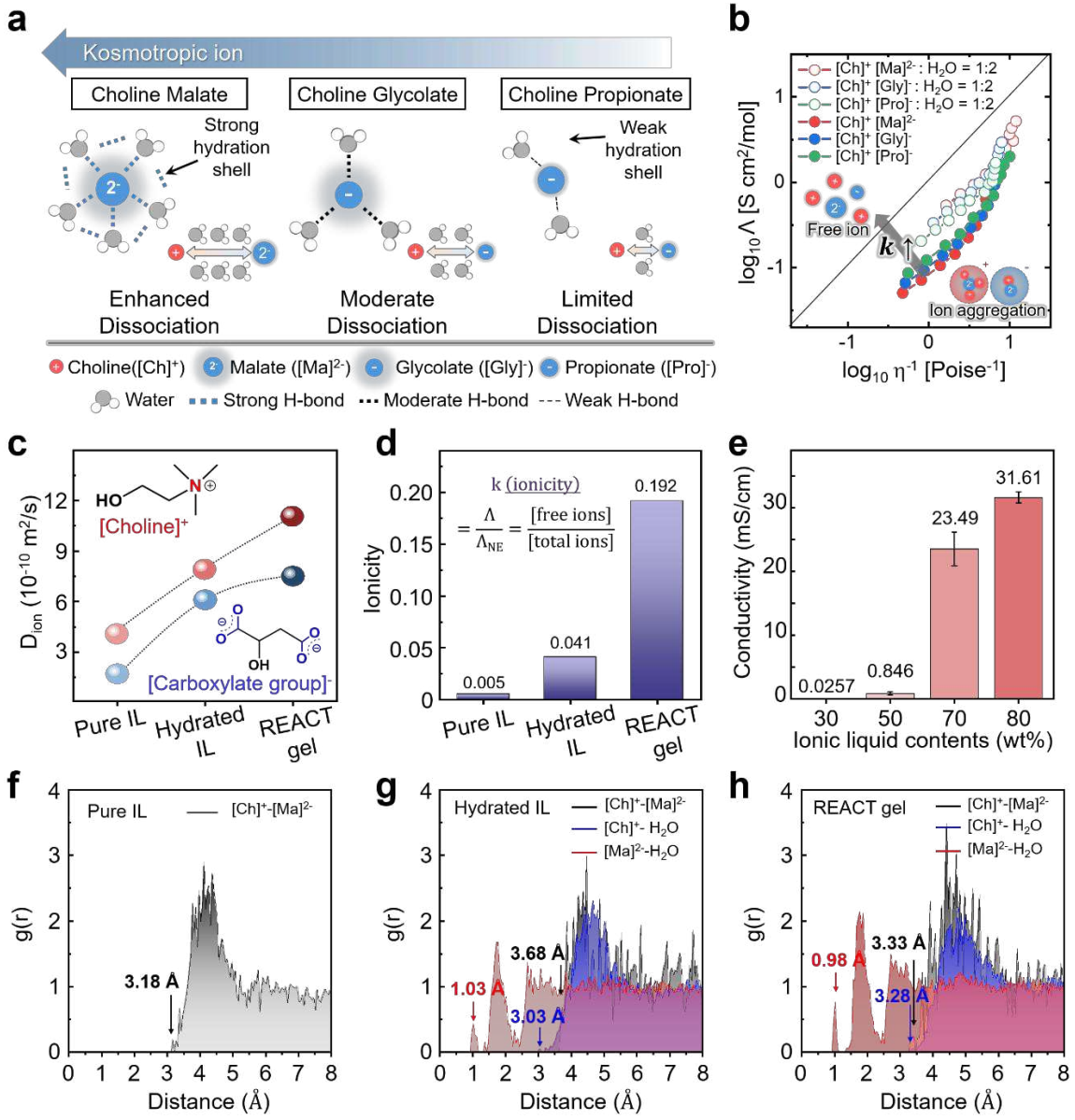


Fig. 2 | Matrix-amplified ion dissociation and transport in REACT gels. a, Schematic illustration of kosmotropic anion-dependent ion dissociation in choline-based ionic liquids. Malate, glycolate and propionate anions were compared to examine how ion-water interactions regulate ion-cluster dissociation. **b,** Walden plot of neat and hydrated ionic liquids. Water addition shifts the ionic liquids toward the ideal Walden line, indicating enhanced ion dissociation. **c,** PFG-NMR-derived diffusivities of choline and malate-derived carboxylate species. Ion diffusivity increases sequentially from the neat ionic liquid to the hydrated ionic liquid and the REACT gel. **d,** Calculated apparent ionicity of choline malate-based systems. The REACT gel shows a marked increase in the free-ion fraction compared with the neat ionic liquid and the hydrated ionic liquid. **e,** Ionic conductivity of REACT gels with different ionic liquid contents. The gels retain stable ionic liquid incorporation and reach a maximum ionic conductivity of approximately 32 mS cm^{-1}. **f-h,** Radial distribution function (RDF) analysis of ion-ion and ion-water correlations in **f,** neat ionic liquid, **g,** hydrated ionic liquid and **h,** hydrated ionic liquid containing one collagen molecule. The black, blue and red lines represent

$[Ch]^+$-$[Ma]^{2-}$, $[Ch]^+$-H_2O and $[Ma]^{2-}$-H_2O correlations, respectively.

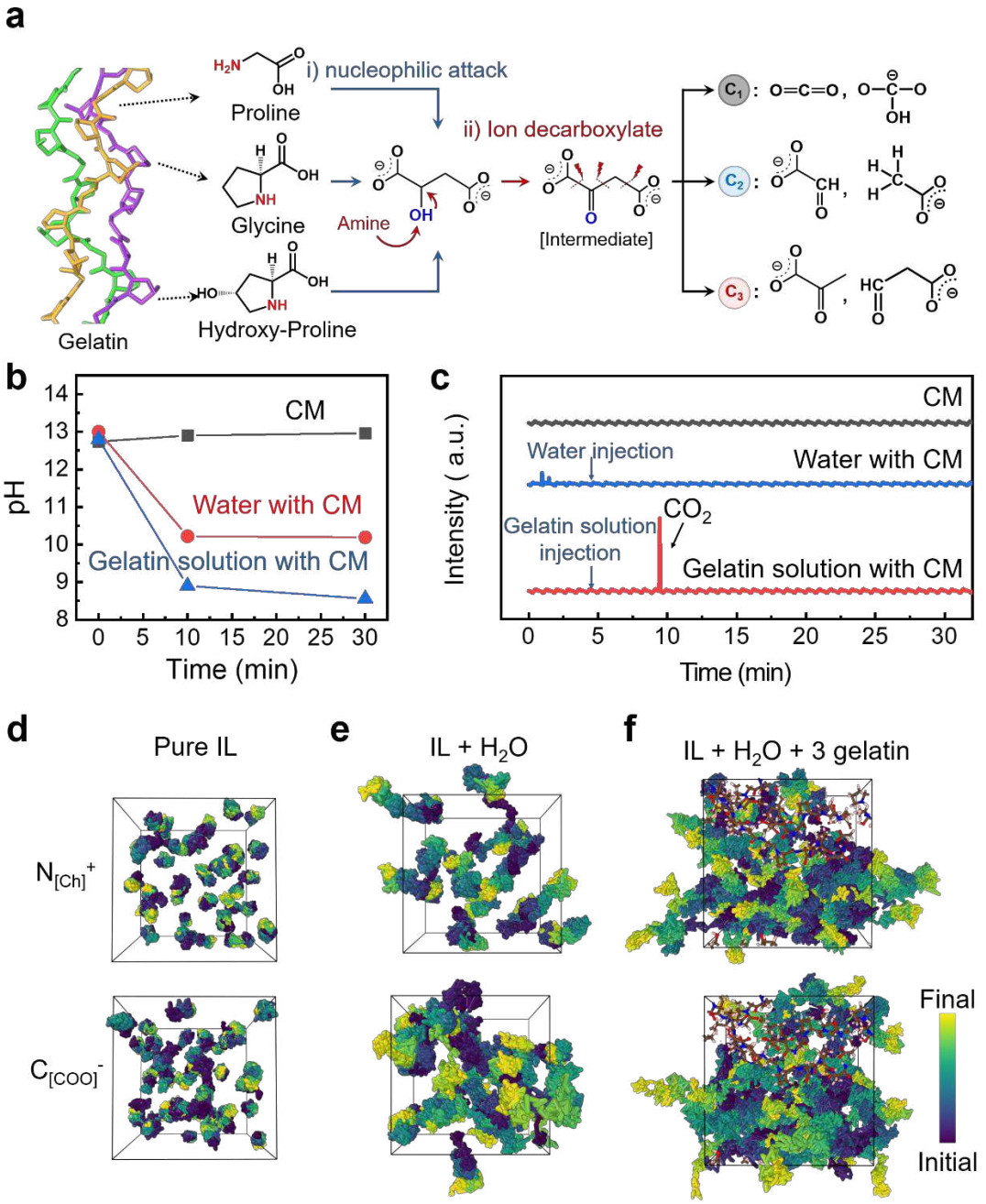


Fig. 3 | Reaction-driven ionic remodeling in REACT gels enhances ion transport. **a,** Schematic illustration of decarboxylation-driven remodeling of malate anions in the gelatin matrix. Nucleophilic sites (amine groups) in the gelatin-derived environment promote malate decarboxylation, generating smaller ionic species. **b,** pH changes in choline malate-based systems after addition of water or gelatin solution. The gelatin-containing system shows a larger decrease in pH, consistent with enhanced decarboxylation and CO_2 formation. **c,** Real-time CO_2 detection by gas chromatography. A distinct CO_2 signal is observed only after addition of gelatin solution, providing direct evidence for matrix-assisted decarboxylation. **d-f,** Diffusion trajectories of the choline nitrogen atom, N($[Ch]^+$), and the malate carboxyl carbon atoms, C(COO^-), in **d,** neat ionic liquid, **e,** hydrated ionic liquid and **f,** hydrated ionic liquid

containing one collagen model (three gelatin-derived chains). Blue and yellow indicate the initial (t = 0 ns) and final (t = 2 ns) positions during the NVT simulations, respectively.

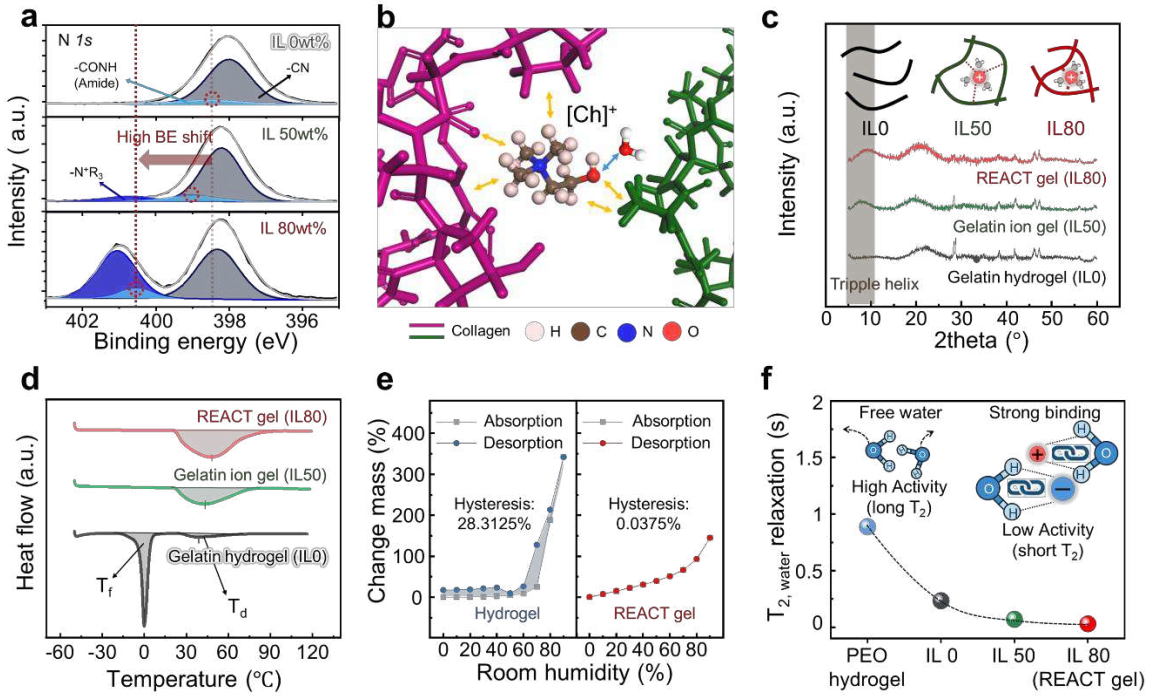


Fig. 4 | Ion-polymer-water networks stabilize REACT gels. a, XPS N 1s spectra of gelatin-based gels with different choline malate contents. The positive binding-energy shifts with increasing ionic liquid content indicate progressively altered nitrogen environments associated with strengthened ion-polymer interactions. **b,** Molecular dynamics snapshot showing choline-mediated electrostatic bridging between collagen chains in the hydrated gelatin matrix. Interfacially confined choline cations occupy interstitial sites between neighboring collagen chains, reinforcing the ion-polymer network. **c,** XRD patterns of gelatin hydrogel, gelatin ion gel and REACT gel. The enhanced low-angle diffraction feature indicates stabilization of ordered gelatin domains in the REACT gel. **d,** DSC thermograms showing enhanced thermal stabilization of the gelatin network in the REACT gel. **e,** Dynamic vapor sorption profiles of the hydrogel and REACT gel during humidity-dependent adsorption and desorption. The reduced mass change and minimal hysteresis of the REACT gel indicate suppressed water exchange with the surrounding environment. **f,** ^{1}H NMR T_2 relaxation analysis of water in gelatin-based gels. The shortened T_2 relaxation time with increasing choline malate content indicates restricted water mobility and stronger water confinement within the ion-water-gelatin network.

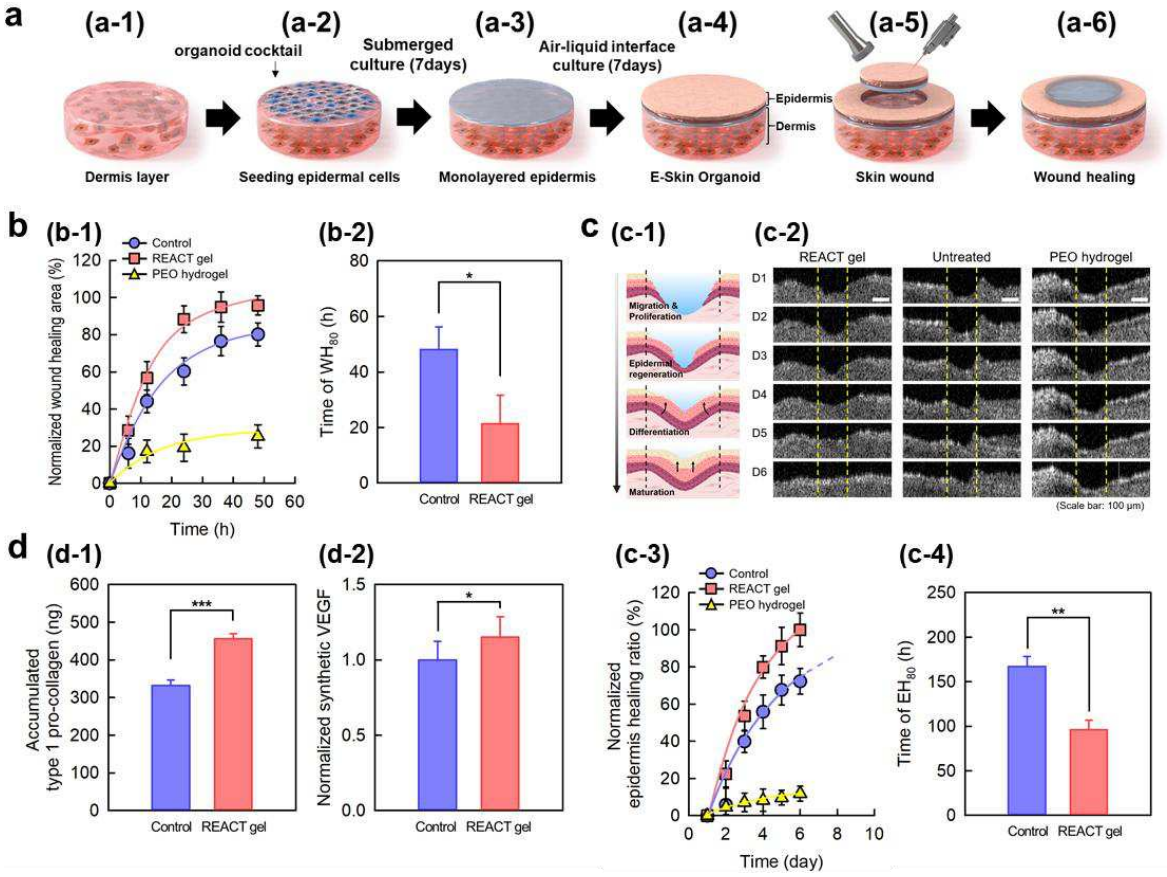


Fig. 5 | REACT gel bioelectronic stimulation promotes wound regeneration in engineered skin organoids. a, Schematic illustration of the engineered skin organoid wound-regeneration model. A dermal matrix was prepared by embedding human dermal fibroblasts (HDFn) within a collagen scaffold (a-1). A cell cocktail containing skin organoids and human epidermal keratinocytes (HEKn) was then seeded onto the dermal layer (a-2), forming a monolayered epidermis (a-3). Epidermal stratification was induced by air-liquid interface culture (a-4). Tissue injury was generated using a biopsy punch or laser irradiation (a-5), followed by application of the ionic gel to evaluate wound regeneration (a-6). **b,** Horizontal wound closure in the engineered skin organoid model. REACT gel (IL80), NaCl-containing hydrogel or no treatment was applied to the wound region, and wound closure was monitored for 48 h. REACT gel stimulation accelerated wound closure, reducing the time required to achieve 80% wound closure (WH_{80}) by approximately 56% compared with the untreated control. **c,** Epidermal regeneration in a laser-induced micro-wound model analyzed by optical coherence tomography (OCT). Schematic illustration of the epidermal regeneration process (c-1). Representative time-resolved OCT cross-sectional images of laser-induced wounds in engineered skin organoids treated with REACT gel, untreated control, and NaCl-containing hydrogel. The dashed lines indicate the wound boundaries (c-2). REACT gel treatment shortened the time required to achieve 80% epidermal reconstruction (EH_{80}) by approximately 43% relative to the control (c-3, c-4). **d,** Biochemical and functional analyses of wound regeneration. REACT gel stimulation increased pro-collagen and VEGF secretion and enhanced angiogenic activity in HUVEC tubule formation assays, including a 94% increase in vascular segment formation compared with the control. Data are presented as mean ± s.d. $P < 0.05$, P < 0.01 and $^{**}P <$ 0.001.

Extended Data

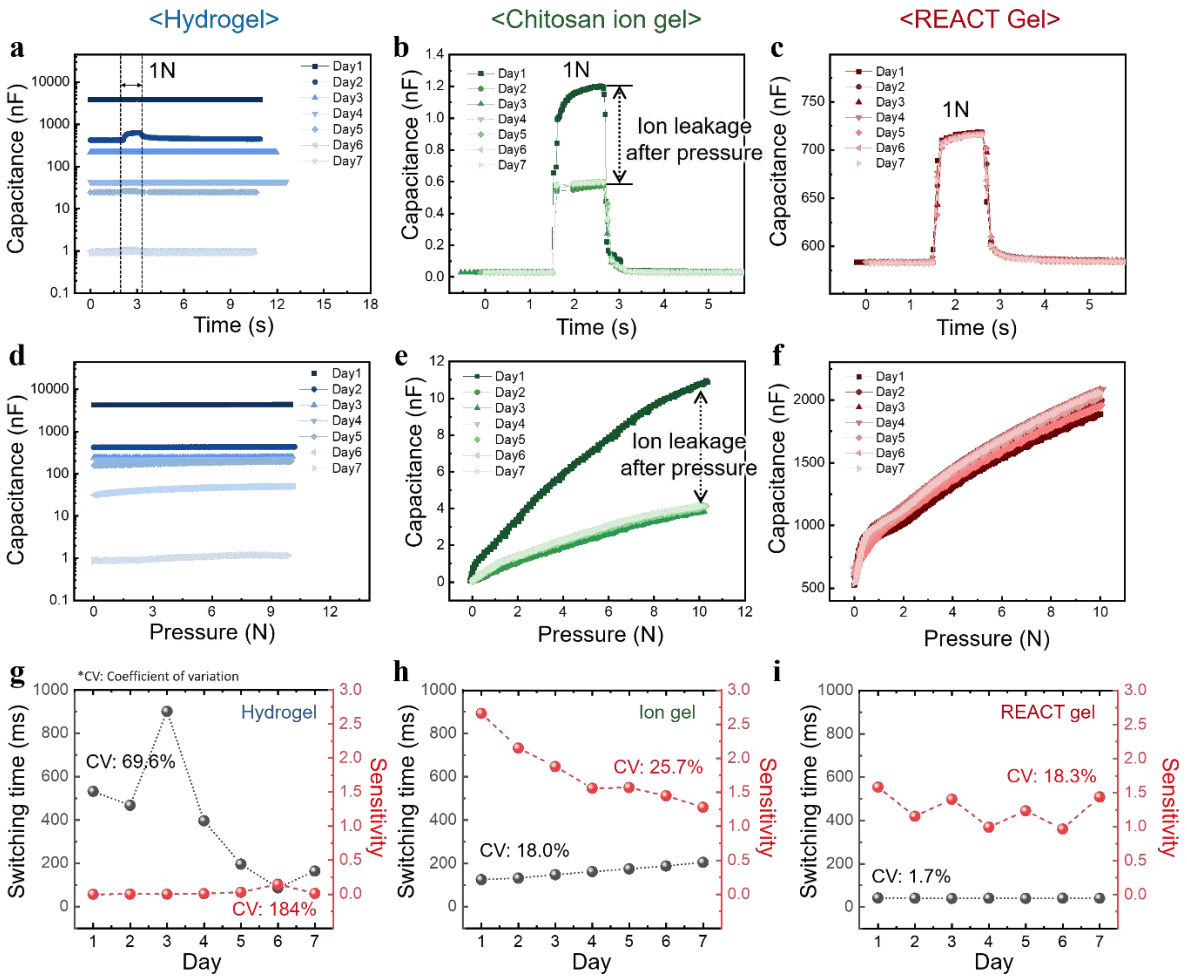
Reaction-driven ionic remodeling enables durable soft electronics

Ji Hong Kim[1]†, Yeongjun Yoon[1]†, Sung Gyu Shin[2]†, Won Hyuk Choi[1], Jong Hwi Kim[1], Yoseph Park[1], Joo Sung Kim[5], Hanbin Choi[6], Hyo Jeong Kim[7], So Young Kim[1], Youngho Eom[7], Jae Hyun Jeong[2*], Kyeounghak Kim[1*], and Do Hwan Kim[1,3,4*]

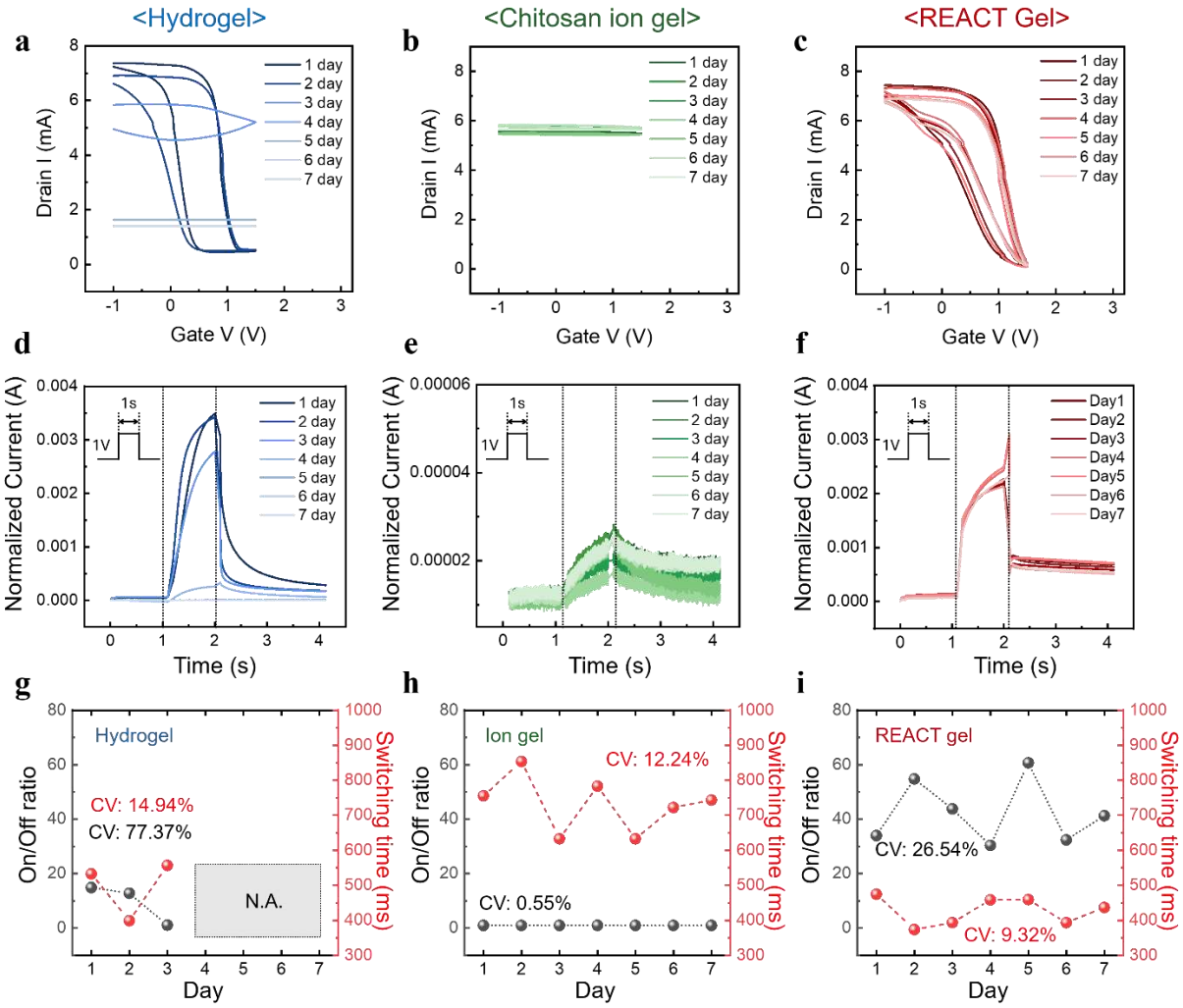
[1]*Department of Chemical Engineering, Hanyang University, Seoul 04763, Republic of Korea.*
[2]*Department of Chemical Engineering, Soongsil University, Seoul, 06978, Republic of Korea.*
[3]*Institute of Nano Science and Technology, Hanyang University, Seoul 04763, Republic of Korea.*
[4]*Clean-Energy Research Institute, Hanyang University, Seoul 04763, Republic of Korea.*
[5]*Thin-Film Device Laboratory, RIKEN, 2-1 Hirosawa, Wako, Saitama 351-0198, Japan.*
[6]*Department of Chemical and Biomolecular Engineering, North Carolina State University, Raleigh, NC, USA*
[7]*Department of Organic and Nano Engineering, Human-Tech Convergence Program, Hanyang University, Seoul 04763, Republic of Korea.*

†These authors contributed equally to this work.

*Corresponding authors' email: nfejjh@ssu.ac.kr (J.H.J.), chemekim@hanyang.ac.kr (K.K.), dhkim76@hanyang.ac.kr (D.H.K.)



Extended Data Fig. 1 | Long-term stability of REACT-based piezocapacitive pressure sensors. a-c, Time-dependent capacitance responses of sensors based on **a,** hydrogel, **b,** chitosan ion gel and **c,** REACT gel under repeated 1 N compression. The hydrogel sensor shows progressive baseline drift, whereas the chitosan ion gel sensor exhibits a gradual reduction in capacitance response. By contrast, the REACT gel sensor maintains a stable and reproducible response during repeated compression. **d-f,** Pressure-dependent capacitance responses of sensors based on **d,** hydrogel, **e,** chitosan ion gel and **f,** REACT gel. The REACT gel sensor exhibits reproducible pressure-dependent capacitance modulation over the tested pressure range. **g-i,** Switching time and sensitivity of sensors based on **g,** hydrogel, **h,** chitosan ion gel and **i,** REACT gel over repeated measurements. The REACT gel sensor shows the smallest variation in sensing performance, with a coefficient of variation in sensitivity of 18.3%.



Extended Data Fig. 2 | Stable ionic gating and switching of REACT gel-based OECTs. a-c, Transfer characteristics of PEDOT OECTs gated with **a,** hydrogel, **b,** chitosan ion gel and **c,** REACT gel over repeated measurements. The hydrogel-gated device shows progressive shifts in transfer characteristics, whereas the chitosan ion gel-gated device exhibits negligible transistor modulation. By contrast, the REACT gel-gated device maintains stable and reproducible transfer characteristics, indicating persistent ionic gating of the PEDOT channel. **d-f,** Transient switching responses of OECTs gated with **d,** hydrogel, **e,** chitosan ion gel and **f,** REACT gel electrolytes. The REACT gel enables rapid and reproducible current modulation, whereas the hydrogel- and chitosan ion gel-gated devices show slower or less stable switching responses. **g-i,** Extracted device response and switching times of OECTs gated with **g,** hydrogel, **h,** chitosan ion gel and **i,** REACT gel electrolytes. The REACT gel-gated OECT maintains stable device response with comparatively short and reproducible switching times during repeated operation.

Supplementary Files

This is a list of supplementary files associated with this preprint. Click to download.

- SupplementaryVideo1.mov
- SupplementaryInformationDoHwanKim.pdf